Journal of Molecular Liquids 387 (2023) 122654

Contents lists available at ScienceDirect

Journal of Molecular Liquids

journal homepage: www.elsevier.com/locate/molliq

Unraveling the Ag^+ ion coordination and solvation thermodynamics in the 1-butyl-3-methylimidazolium tetrafluoroborate ionic liquid

Matteo Busato [a,b,*], Paola D'Angelo [a], Andrea Lapi [a,c], Francesco Tavani [a], Daniele Veclani [a,d], Marilena Tolazzi [b], Andrea Melchior [b,**]

[a] Dipartimento di Chimica, Sapienza Università di Roma, p.le A. Moro 5, 00185, Roma, Italy
[b] Dipartimento Politecnico di Ingegneria e Architettura, Università di Udine, via delle Scienze 206, 33100, Udine, Italy
[c] Istituto per i Sistemi Biologici (ISB-CNR), Sede Secondaria di Roma-Meccanismi di Reazione, c/o Dipartimento di Chimica, Sapienza Università di Roma, p.le A. Moro 5, 00185, Roma, Italy
[d] Istituto per la Sintesi Organica e la Fotoreattività (ISOF-CNR), via P. Gobetti 101, 40129, Bologna, Italy

ARTICLE INFO

Keywords:
Silver
Ionic liquids
Tetrafluoroborate
Molecular dynamics
X-ray absorption spectroscopy
Coordination
Thermodynamics

ABSTRACT

The solvation of the Ag^+ ion in the 1-butyl-3-methylimidazolium tetrafluoroborate ($[C_4mim][BF_4]$) ionic liquid (IL) has been studied by means of experimental and theoretical methods with the aim of elucidating the cation coordination structure and thermodynamic properties. Car-Parrinello molecular dynamics (CPMD) simulations showed that the Ag^+ ion is coordinated by an average number of four $[BF_4]^-$ anions in a pseudo-tetrahedral geometry. A high configurational disorder of the first solvation sphere is found, where the anions can be found both in mono- and bidentate coordination mode around the Ag^+ ion. Also, a solvational equilibrium is observed as due to $[BF_4]^-$ anion dissociation along the trajectory. The analysis of X-ray absorption spectroscopy data confirmed the picture provided by the CPMD simulation. Classical molecular dynamics simulations were carried out to obtain the single-ion solvation thermodynamic parameters. The negative water → IL free energy of transfer suggests that the Ag^+ ion is more favorably solvated in the $[C_4mim][BF_4]$ IL than in water. This behavior is due to a balance between the enthalpic and entropic contributions, which allows to find a rationale to the strong solvation capabilities of BF_4-based ILs towards Ag^+.

1. Introduction

Ionic liquids (ILs) have attracted much attention as a more sustainable alternative to traditional organic solvents owing to key-properties like a practically negligible vapor pressure, non-flammability, thermal and electrochemical stability, and good solvation ability for both neutral and charged species [1]. Due to such attractive features, ILs emerged as new media for a variety of applications such as selective extractions [2–4], energy storage devices [5,6], electrochemical depositions [7,8], and catalytic reactions [9], among others. As numerous of these applications also involve the presence of dissolved metal ions in IL phases, in recent years several studies aimed at defining the structure of the solvates and their complexes have been carried out [10–15].

As far as the Ag^+ ion is concerned, several studies were focused on the selective recovery of this metal from complex aqueous matrixes [16–20] and electrodeposition processes [21–23] using ILs. Moreover, great interest has arisen from the application of dissolved Ag^+ salts in the petrolchemical industry for the olefin/alkane separation. The latter process is not trivial, due to the similar molecular weights and volatility of the compounds to be separated. Current industrial separation methods consist in cryogenic distillation, which has high costs and energy consumption as major drawbacks [24]. To develop more sustainable processes, ILs have been proposed in extractive distillation [25,26] and as media for facilitated transport in immobilized liquid membranes. Such systems exploit the ability of dissolved Ag^+ ions to selectively and reversibly bind olefins by means of π-complexation [27–31]. Liquid phases containing Ag^+ in 1-butyl-3-methylimidazolium tetrafluoroborate ($[C_4mim][BF_4]$) have been employed in olefin/alkane separation as either free liquid phase or immobilized on membranes [30,32]. In this context, several studies [29,33,34] showed a strong dependence of the olefin binding affinity, absorption capacity, as well as stability towards metal reduction upon the nature of the Ag^+ salt, IL type and of the

* Corresponding author at: Dipartimento di Chimica, Sapienza Università di Roma, p.le A. Moro 5, 00185, Roma, Italy.
** Corresponding author at: Dipartimento Politecnico di Ingegneria e Architettura, Università di Udine, via delle Scienze 206, 33100, Udine, Italy.
E-mail addresses: matteo.busato@uniroma1.it (M. Busato), andrea.melchior@uniud.it (A. Melchior).

https://doi.org/10.1016/j.molliq.2023.122654
Received 5 April 2023; Received in revised form 5 July 2023; Accepted 22 July 2023
Available online 28 July 2023

molar composition of the solutions. The results obtained indicate that the metal solvation (number of coordinated anions, binding strength) in the starting IL solution is a key-factor in determining the performance of the separation system. Therefore, studies aiming at deepening the knowledge about the Ag^+ ion speciation and solvational properties in ILs could improve the understanding of the fundamental processes at the base of separation process.

The Ag^+ ion coordination in non-aqueous solutions has been the subject of numerous structural [35–37] and thermodynamic [38–44] studies. The Ag^+ ion presents a variable coordination in solution, which is tetrahedral in non-aqueous solvents [35,45], and nearly linear ("2+2") in water, as recently shown by means of X-ray absorption spectroscopy (XAS), large-angle X-ray scattering, and Car-Parrinello molecular dynamics (CPMD) simulations [35,46]. On the contrary, only few works about the Ag^+ ion coordination in ILs have been carried out. By means of first-principles simulations, it was found that the Ag^+ ion has a flexible and disordered solvation structure in 1-ethyl-3-methylimidazolium trifluoromethanesulfonate [C_2mim][TfO] with a coordination number (CN) ranging from 2 to 4 [47]. In another recent study [48], the solvation structure in N-butyl-N-methylpyrrolidinium dicyanamide ([C_4pyr][DCA]) was investigated by means of attenuated total reflectance-ultraviolet spectroscopy and classical molecular dynamics simulations, which provided a CN of ~5.

As for the solvation thermodynamics, the Ag^+ ion free energies of transfer from dimethylsulfoxide (DMSO) to several ILs (ΔG_{trans}(DMSO →IL)), including 1-ethyl-3-methylimidazolium tetrafluoroborate ([C_2mim][BF_4]), [C_4mim][BF_4], and those based on the 1-ethyl-3-methylimidazolium and 1-butyl-3-methylimidazolium cations with the bis(trifluoromethylsulfonyl)imide anion ([C_2mim][Tf_2N] and [C_4mim][Tf_2N], respectively) have been obtained by potentiometric measurements [49,50] (Table S1). The combination of these data with the single-ion Gibbs free energy of hydration (ΔG_{hyd}) [51,52] and transfer from water to DMSO (ΔG_{trans}(water→DMSO)) [52] (Table S1) allows one to calculate the ion solvation free energy in the IL (ΔG_{solv}) through the thermodynamic cycle depicted in Scheme S1 and ultimately the free energy for the transfer process from water to the IL solution (ΔG_{trans}(water→IL)). All these data, together with those calculated for the Zn^{2+} ion [49,50], taken for the sake of comparison as representative of the divalent state are collected in Table 1 and S1.

The positive ΔG_{trans}(water→IL) for the Zn^{2+} ion in ILs containing the $[Tf_2N]^-$ anion was explained by the weak coordination strength of the $[Tf_2N]^-$ anion [10,11,14,15]. On the other hand, the trend seems to be reversed for ILs carrying the $[BF_4]^-$ anion (Table 1). The situation becomes even more intriguing when the Ag^+ ion is considered, as its transfer is not only favorable towards the BF_4-based ILs, but appears to be only slightly unfavorable or even favorable in the Tf_2N-based ones. This peculiar behavior shows how the relationship between metal ion solvates and ILs is strictly system-dependent, leaving space for further investigation.

In this work, we tackle some of these open questions by proposing a study on the solvation of the Ag^+ ion in the [C_4mim][BF_4] IL by a combined approach based on CPMD, classical MD simulations, and XAS experiments. First-principles MD techniques have previously shown to be necessary to describe the often complex coordination of this metal ion in molecular solvents [46,47,53,54], while the XAS technique has long been a working horse for the study of metal ions coordination in liquid systems due to its unique sensitivity towards the closest environment of the photoabsorber [35,36,55,56]. After having obtained a robust model for the Ag^+ ion coordination in solution, we employed classical MD simulations to retrieve crucial thermodynamic quantities for the description of the metal ion solvation in [C_4mim][BF_4] and in particular for its transfer process from water. Note that in this case we switched to an empirical interaction potential due to the high computational cost of a first-principles treatment, which prevents the simulation of system sizes able to satisfy the infinite dilution condition required by the estimation of thermodynamic state functions. We envisage that the study about the peculiar relationship between the Ag^+ ion solvate and the [C_4mim][BF_4] IL could provide new tools for a more conscious employment of ILs as advanced processing media and possibly expand the State-of-the-Art view about these inherently complex systems.

Table 1
Gibbs free energies (kcal mol^{-1}) for the Zn^{2+} and Ag^+ ion transfer from water to ILs at 298 K obtained from literature experimental data.†

IL	ΔG_{trans}(water→IL)	
	Zn^{2+}	Ag^+
[C_2mim][Tf_2N]	10.2	0.5
[C_4mim][Tf_2N]	10.0	-4.4
[C_2mim][BF_4]	-18.2	-16.8
		-6.5
[C_4mim][BF_4]	-12.0	-12.4
		-4.0

† The ΔG_{trans}(water→IL) is calculated as ΔG_{solv}(IL) - ΔG_{hyd} from the values reported in Table S1 [49–52].

2. Materials and methods

2.1. CPMD simulation

The *ab initio* MD simulation of the Ag^+ ion in [C_4mim][BF_4] has been carried out with the Car-Parrinello approach by means of the CPMD v.4.3 code [57]. The BLYP functional has been employed with Grimme's DFT-D2 empirical dispersion corrections [58]. Norm-conserving pseudopotentials of the Troullier-Martins type were used for all atoms. Kohn-Sham orbitals for valence electrons were expanded in plane-waves with a cutoff energy of 80 Ry. Energy expectations were calculated in reciprocal space using the Kleinman-Bylander transformation [59]. A fictitious mass of 400 a.u. was associated to the electronic degrees of freedom and a time step of 4 a.u. (0.097 fs) was employed. The relative small fictitious mass of 400 a.u. was previously suggested by G. Galli et al. [60,61] to improve the bulk water description and, along with the whole level of theory here employed, provided a good reproduction of metal ion coordination in aqueous solution [62–65], in particular for what concerns the Ag^+ ion [46].

One Ag^+ ion was set in the middle of a periodic cubic box of 16.42 Å edge and surrounded by 14 $[C_4mim]^+$ and 15 $[BF_4]^-$ ions. This number of species and box dimension were chosen to reproduce the pure IL density [66]. This system was pre-equilibrated with a 10 ns MD run in NVT conditions with a classical potential (*vide infra*). In this simulation, a temperature ramp of 2 ns was employed to bring the system from 298 to 500 K, then a high-temperature run was carried out for 6 ns, and the system was then simulated at 298 K for additional 2 ns. For the CPMD simulation a wave-function optimization was followed by a 2 ps equilibration in the NVE ensemble and by a further equilibration in NVT conditions at 500 K for 10 ps. High-temperature equilibrations were previously observed to be required for slow-dynamics liquids like ILs [10–12,67]. The production run for data collection was carried out for 50 ps in the NVT ensemble at 298 K. The temperature of the nuclei was kept constant by coupling the ionic subsystem to the Nosé-Hoover thermostat with a coupling frequency of 1500 cm^{-1}. No thermostat was associated to the electronic degrees of freedom. The fictitious electron kinetic energy was constantly monitored during the simulation and showed no relevant drifts. The VMD 1.9.3 software [68] was employed for trajectories visualization and the TRAVIS program [69] for the analysis.

2.2. Classical MD simulations

The system for the classical MD simulations consisted in one Ag^+ ion in 199 $[C_4mim]^+$ cations and 200 $[BF_4]^-$ anions with an initial side length of 39.01 Å. The number of species and box dimensions were chosen to reproduce the pure IL density and infinite dilution conditions for the metal ion [66]. Starting geometries were built by randomizing the atom positions with the PACKMOL package [70]. The structure and interactions of the $[C_4mim][BF_4]$ IL were represented by the all-atom non-polarizable force field developed by Canongia Lopes and Padua [71] with the Lennard-Jones (LJ) parameters of the $[BF_4]^-$ anion taken from Liu et al. [72]. The LJ parameters employed for the Ag^+ ion were developed in this work and are $\sigma_{Ag} = 1.50$ Å and $\epsilon_{Ag} = 9.5602\times10^{-2}$ kcal mol^{-1}. Details about the generation of this interaction potential are given in the Supplementary Material (SM). After an energy minimization, the system was equilibrated in the NVT ensemble with a temperature ramp going from 298 to 700 K, staying at high temperature for 10 ns, and gradually cooling down and keeping at 298 K for further 10 ns. Then a 10 ns NPT equilibration at 298 K and 1 atm was carried out. The temperature was controlled with the thermostat implicitly handled by the stochastic dynamics leap-frog integrator with a coupling constant of 0.5 ps, while in NPT conditions the pressure was coupled to the Parrinello-Rahman barostat with a relaxation constant of 1.0 ps. A 1.0 fs timestep has been employed for all simulations and the stretching vibrations involving the hydrogen atoms were constrained with the LINCS algorithm. All calculations have been performed with the Gromacs 5.1.4 program [73].

Free energy calculations for the Ag^+ single-ion solvation in the $[C_4mim][BF_4]$ IL were carried out with a free energy perturbation method. The free energy difference for bringing the system from the initial to the final state has been represented as a function of a decoupling parameter λ, which multiplies the non-bonded part of the metal ion interaction potential. To this purpose, 15 λ windows were chosen to change from $\lambda = 0$ (non-interacting metal ion) to $\lambda = 1$ (fully interacting metal ion). The first 5 λ values correspond to turning on the LJ interactions, while the successive 10 are related to the electrostatic part represented by a Coulomb potential. This number of windows has been previously demonstrated to provide a good estimation of the Co^{2+} and Zn^{2+} ion free energy of hydration and solvation in the $[C_4mim][Tf_2N]$ IL, in agreement with experimental data [10,11]. For each λ value, an NPT run was performed for 15 ns at 298 K and 1 atm and the first 5 ns were discarded as equilibration time. The final free energy value has been calculated with the Bennett Acceptance Ratio method [74]. Free energy calculations at different temperatures were also performed to obtain the solvation enthalpic and entropic terms. This protocol has turned out to be the most accurate for the calculation of the entropy change for metal ions in water [10,11,75,76]. To this purpose, the same protocol described above has been applied at five different temperatures in the 298 - 420 K range.

To obtain the free energy for the transfer process of the Ag^+ ion from water to the $[C_4mim][BF_4]$ IL, free energy calculations were also performed in aqueous solution. The system consisted of one Ag^+ ion in 600 SPC/E water molecules, with an initial side length of 26.21 Å chosen to reproduce pure water density and infinite dilution conditions for the metal ion. The system was first minimized and equilibrated in NVT conditions at 298 K for 10 ns, then for the ΔG_{hyd} calculation 15 λ windows were employed. For each λ value, 2 ns equilibrations and 5 ns runs for data collection were performed in NPT conditions at 298 K and 1 atm. Hydration enthalpy and entropy were obtained by free energy calculations at five different temperatures in the 280 - 360 K range with the same simulation protocol.

2.3. XAS measurements

$[C_4mim][BF_4]$ was purchased from Iolitec GmbH (Germany) with a stated purity of 99% and dried under vacuum at 50 °C for 36 h prior use, while $AgBF_4$ (99%) from Fisher Scientific (Milan, Italy). A 0.1 M solution of $AgBF_4$ in $[C_4mim][BF_4]$ was prepared by adding a stoichiometric amount of the salt into the IL. The resulting solution was sonicated until complete dissolution of the metal salt and then dried under vacuum for 36 h at 50 °C. Ag K-edge XAS data were collected in transmission mode at the 11.1 XAFS beamline [77] of Elettra-Sincrotrone Trieste (Italy). Standard cells for liquids with Kapton windows were filled with the liquid sample and kept under N_2-flux during data acquisition to avoid contact with the air moisture. The measurements were performed with a Si(311) double-crystal monochromator, while the storage ring was operating at 2 GeV and the beam current was between 200 and 300 mA. Energy calibration was carried out by assigning the first inflection point of the K-edge spectrum of metallic Ag to 25516.5 eV. Three spectra were recorded and averaged for each sample.

2.4. EXAFS data analysis

The analysis of the EXAFS (extended X-ray absorption fine structure) region of the absorption spectrum collected on the $AgBF_4$ salt and on the 0.1 M $AgBF_4$ solution in $[C_4mim][BF_4]$ was carried out with the GNXAS program [78,79]. The amplitude function $A(k,r)$ and phase shifts $\phi(k,r)$ have been calculated from clusters with fixed geometry with muffin-tin (MT) potentials and advanced models for the exchange-correlation self-energy (Hedin-Lundqvist), which allow one to take into account the photoelectron inelastic losses intrinsically [80]. The MT radii were chosen to obtain a ~20% overlap of the MT spheres and were 1.91, 0.90, and 0.80 Å for the Ag, F, and B atoms, respectively. Theoretical signals associated with n-body distribution functions have been calculated within the multiple-scattering (MS) theory and summed in order to reconstruct the total theoretical contribution [81].

The EXAFS spectrum of solid $AgBF_4$ was analyzed starting from its crystallographic structure [82]. The MT cluster was built from the $AgBF_4$ crystal by selecting a radius of 6 Å from the photoabsorber with the ATOMS code [83]. Single-scattering (SS) theoretical signals were grouped to take into account the four fluorine atoms closest to the silver center (Ag-F^{1st}), two fluorine atoms at a slightly longer distance (Ag-F^{2nd}), four and two fluorine atoms set at even longer distances (Ag-F^{3rd} and Ag-F^{4th}, respectively), plus an Ag-B contribution representing the boron atoms of the seven $[BF_4]^-$ anions surrounding the metal center [82]. The EXAFS data of the 0.1 M $AgBF_4$ solution in $[C_4mim][BF_4]$ were analyzed starting from the model provided by the CPMD results (*vide infra*). The MT cluster was a tetrahedral $[Ag(BF_4)_4]^{3-}$ unit and a SS Ag-F theoretical signal accounting for the first-shell fluorine atoms has been calculated together with a Ag-B SS signal connected with the second-shell boron atoms of the coordinating $[BF_4]^-$ anions. In both the solid state and liquid system analysis, each two-body distribution has been modeled as a Γ-like function depending on four structural parameters, namely the coordination number N, the average distance R, the Debye-Waller factor σ^2, and the asymmetry index β, which have been optimized during the fitting procedure to obtain the best agreement with the experimental data, with the exception of the coordination numbers for the $AgBF_4$ solid that have been kept fixed to the crystallographic structure. Least-squares minimizations have been carried out on the raw data directly, without preliminary background subtraction or Fourier filtering, by optimizing all the structural parameters. Non-structural parameters have been also optimized, namely the Ag K-edge ionization energy E_0, and the energy positions and amplitudes of the double-electron excitation channels $KN_{2\&3}$, KN_1, and $KM_{4\&5}$. The inclusion of the double-excitations allowed us to keep the amplitude reduction factor S_0^2 constrained between 0.95 and 1.00.

3. Results and discussion

3.1. Ag^+ ion coordination in $[C_4mim][BF_4]$: CPMD results

CPMD simulations have been carried out to get insights into the Ag^+ ion coordination in the $[C_4mim][BF_4]$ IL. To this purpose, site-site ra-

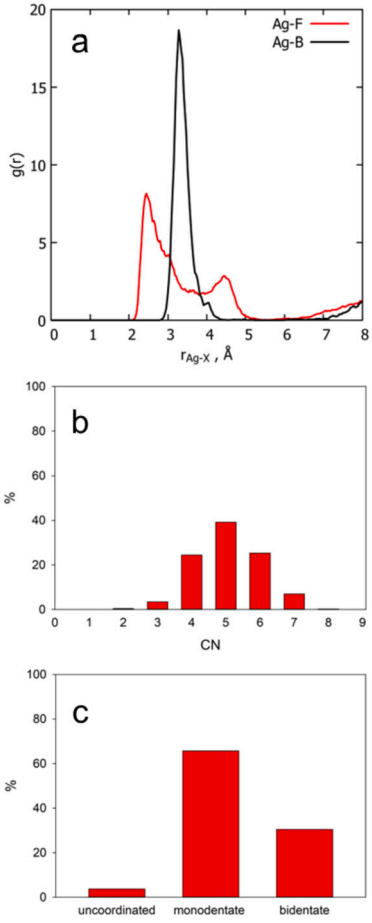

Fig. 1. a) Ag-F and Ag-B radial distribution functions $g(r)$'s, b) instantaneous Ag-F coordination number and c) coordination mode of the of $[BF_4]^-$ anions distributions (3.0 Å cutoff) calculated from the CPMD simulation of the Ag^+ ion in $[C_4mim][BF_4]$.

dial distribution functions $g(r)$'s have been computed for the Ag-F and Ag-B pairs and the obtained curves are reported in Fig. 1a. The Ag-F $g(r)$ shows a broad distribution with a first maximum located at 2.45 Å. This value is significantly shorter than the Ag-F distance determined for the $AgBF_4$ salt from X-ray diffraction analysis (2.561(4) - 2.950(2) Å) [82], suggesting a contraction of the Ag-F bond in IL solution in comparison with the solid state. The shape of the Ag-F $g(r)$ shows a saddle point corresponding to a distance of ~3.0 Å, and integration of the curve up to this cutoff value delivers a coordination number of 5.3 fluorine atoms. An additional minimum after the first broad peak is observed at a ~3.5 Å distance and gives back a coordination number of 7.6 fluorine atoms. Furthermore, a second maximum is located at 4.46 Å. The latter contribution can be associated to the non-coordinating external fluorine atoms of the $[BF_4]^-$ anions, and integration of the Ag-F $g(r)$ after this maximum gives a total number of 16 fluorine atoms. As concerns the Ag-B $g(r)$, contrarily to the Ag-F one, this distribution shows a single and well defined peak with a maximum at 3.28 Å integrating 4.0 boron atoms. The whole result indicates that an average number of four $[BF_4]^-$ anions is present in the Ag^+ first solvation sphere. This situation is different from that obtained for the solid state, as it was found that the Ag^+ cation is coordinated by 10 fluorine atoms belonging to seven different $[BF_4]^-$ anions [82]. In the liquid system, the broad shape of the Ag-F distribution and the absence of a well-defined first peak suggests a fluxional situation where each of the four $[BF_4]^-$ anions can coordinate with more than one fluorine-donor atom. To obtain more insights into this tendency, we computed the instantaneous Ag-F coordination number up to a cutoff distance of 3.0 Å (Fig. 1b). This cutoff has been selected on the basis of the solid state structure [82] where fluorine atoms are located between 2.561 and 2.950 Å from the Ag^+ ion. As a result, the number of fluorine atoms shows a wide distribution with a major fraction included in the 4-6 range. The reason of this result can be better appreciated from the distribution of the coordination mode of the $[BF_4]^-$ anions (Fig. 1c), which results to be either mono- (~66%) or bidentate (~30%). It should be noted that in a small percentage (~4%) of the solvated Ag^+ ion structures the $[BF_4]^-$ result uncoordinated, that is, all fluorine atoms of one anion are located beyond the 3.0 Å cutoff. The latter finding suggests that dissociation of the anions could occur during the trajectory. To get more details about this process, the time evolution of the Ag-B distances during the CPMD trajectory is reported in Fig. 2. It can be observed that during most of the simulation the Ag-B distances lie in the 3.42 ± 0.25 Å range, corresponding to coordinating $[BF_4]^-$ anions (as an example, see snapshot B in Fig. 2). However, several dissociation events occur corresponding to significantly longer Ag-B distances and evidenced by A and C snapshots where one $[BF_4]^-$ anion leaves the Ag^+ coordination sphere (Fig. 2). Note that these two events were observed for a simulation time of 50 ps, which is consistent with the computational effort required by *ab initio* MD simulations, but represents an inevitably short time as compared to the usually observed lifetimes of solvation complexes [67]. This result delivers a fluxional picture where a high amount of configurational disorder is present in the Ag^+ solvation sphere, both because of $[BF_4]^-$ anions occasionally changing their coordination mode and because of the existence of the $[Ag(BF_4)_4]^{3-} \rightleftharpoons [Ag(BF_4)_3]^{2-} + [BF_4]^-$ solvational equilibrium. This labile coordination environment of the Ag^+ ion has been previously observed in a first-principles simulation study [84] on a hypothetical IL $[Ag(C_2H_4)][BF_4]$ where it was shown that $[BF_4]^-$ anions were able to coordinate either as mono- or bidentate and that ligand exchanges were detected at high temperatures (514 and 617 K) despite the short simulation time (5 ps).

Combined distribution functions (CDFs) for the Ag-X distances and X-Ag-X angles (X = F, B) have been also computed to get more insights into the geometry of the $[BF_4]^-$ anions around the Ag^+ ion. The CDF associated to the Ag-F distances and F-Ag-F angles (Fig. 3a) covers a broad angle distribution centered at ~111°, while the Ag-F distance distribution corresponds to the first maximum of the Ag-F $g(r)$ (Fig. 1a). The angular distribution spans into a range of ±10° if a normalized probability cutoff of ≥ 0.8 is considered for the CDF values. This result is consistent with the observed dynamic coordination with mobile fluorine atoms. On the other hand, the CDF relative to the Ag-B distances and B-Ag-B angles (Fig. 3b) presents a more defined high probability spot centered at ~115° and 3.28 Å with a narrow probability distribution, consistent with a pseudo-tetrahedral geometry of the coordinating $[BF_4]^-$ anions.

3.2. Ag^+ ion coordination in $[C_4mim][BF_4]$: XAS results

XAS data have been collected on a 0.1 M $AgBF_4$ solution in the $[C_4mim][BF_4]$ IL and, for the sake of comparison, on the $AgBF_4$ salt. The obtained spectra are shown in Fig. 4. The coordination of the Ag^+ ion in the $AgBF_4$ crystal has been previously determined on the basis of the crystallographic structure reported in the literature [82]. The metal polyhedron was found to share edges with three and apexes with four $[BF_4]^-$ units, and each silver center is surrounded by 10 fluorine atoms at 2.561(4) - 2.950(2) Å and 7 boron atoms at 3.367 - 3.913 Å distances. As a result, three $[BF_4]^-$ anions are connected to the metal ion *via* two fluorine atoms. In Fig. 4a we report the comparison between the XANES (X-ray absorption near edge structure) spectra collected on solid $AgBF_4$ and on the IL solution. The obtained profiles present marked differences after the edge region. As the low-energy part of the absorption spectrum is known to be very sensitive to the three-dimensional arrangement of the scattering atoms around the photoabsorber [46,67], this result suggests a different coordination of the $[BF_4]^-$ anions towards the Ag^+ center in the IL solution with respect to the solid state. In addition, the

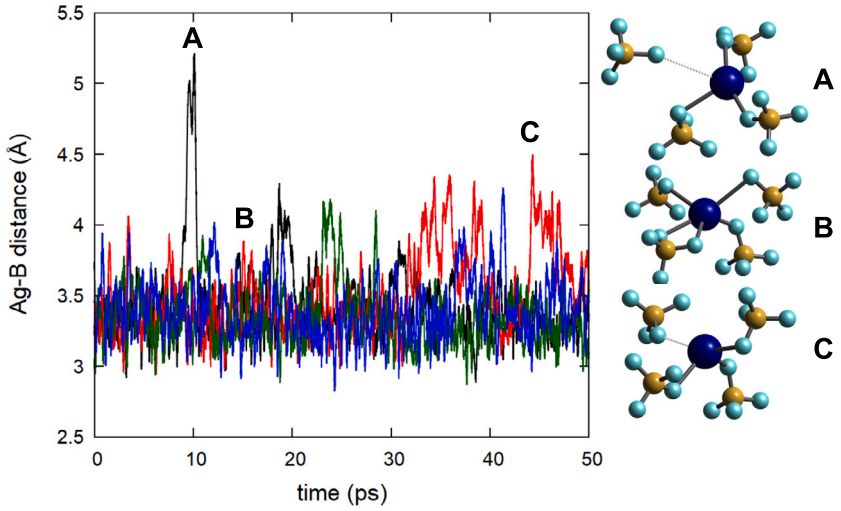

Fig. 2. Time evolution of the distances between the Ag^+ ion and the B atom of the coordinating $[BF_4]^-$ anions calculated from the CPMD simulation of the Ag^+ ion in $[C_4mim][BF_4]$. On the right three snapshots representative of different coordination of BF_4^- anions are reported. In A) and C) the dissociation of one BF_4^- anion is shown. The dotted lines connect Ag^+ ion to the closest F atom of the dissociated BF_4^- anion, which correspond to 3.77 and 3.27 Å in A and C, respectively. In snapshot B, a representative structure of one $Ag[BF_4]_4^{3-}$ solvate where 5 F atoms from the four BF_4^- anions are coordinated to the metal ion is shown.

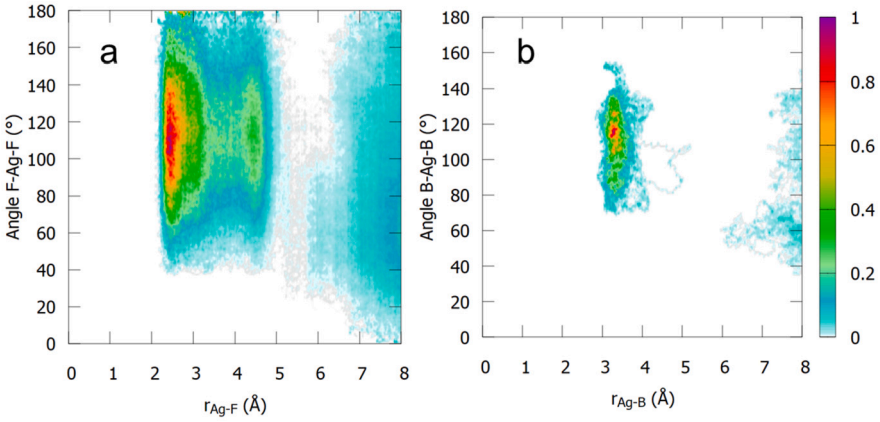

Fig. 3. Combined distribution functions (CDFs) between a) Ag-F distances and F-Ag-F angles and b) Ag-B distances and B-Ag-B angles calculated from the CPMD simulation of the Ag^+ ion in $[C_4mim][BF_4]$. The values represented by the color-code on the right refer to the normalized relative probability of finding a particle at that distance and angle from the reference.

frequency of the main oscillation is higher in case of the $AgBF_4$ salt with respect to the $[C_4mim][BF_4]$ solution, suggesting the presence of scattering centers at shorter distances in the latter case. To better appreciate this difference, the EXAFS spectra were extracted from the raw data, and the obtained profiles are shown in Fig. 4b. Inspection of these curves shows that the frequency of the main EXAFS oscillation of the IL solution is lower, confirming that the Ag-F coordination distance is shorter in the IL as compared to the solid state, in agreement with the CPMD simulation results (Fig. 1a). This finding is confirmed by the corresponding Fourier transformed (FT) spectra calculated in the 1.0 - 8.7 $Å^{-1}$ k-range, where the first peak is found at shorter distances for the $AgBF_4$ solution in the $[C_4mim][BF_4]$ IL (Fig. 4c). This instance is not surprising, as the local environment around a metal center in a solid state structure can differ significantly from what is found for a disordered liquid system [85].

The analysis of the EXAFS data has been carried out to obtain a more quantitative determination of the local structure around the Ag^+ ion. First, we analyzed the EXAFS part of the absorption spectrum recorded on solid $AgBF_4$ starting from its crystallographic structure [82]. A least-squares fit was carried out in the 2.9 - 12.0 $Å^{-1}$ k-range and the best-fit results are shown in the upper left panel of Fig. 5. Here, the theoretical two-body signals are depicted together with the total theoretical contribution compared with the experimental data. As can be observed, a good agreement between the theoretical and the experimental data is obtained, as is also evident from the corresponding FT spectra shown in the lower left panel of Fig. 5. The FT's have been calculated in the 2.9 - 12.0 $Å^{-1}$ range. The complete list of the optimized structural parameters is reported in Table 2, while the E_0 value resulted to be 3.1 eV above the first inflection point of the experimental spectrum. The results of the EXAFS analysis are therefore fully compatible with the local structure of the Ag^+ ion in solid $AgBF_4$ as determined by its crystallographic structure [82], corroborating the goodness of the employed protocol.

The EXAFS data collected on the $[C_4mim][BF_4]$ solution have been analyzed to determine the Ag^+ ion coordination after the dissolution of the $AgBF_4$ salt in the IL. In a first step, this analysis was carried out starting from the local structure of the Ag^+ ion in the $AgBF_4$ crystal, to verify if a change in the metal ion coordination occurs by passing from the solid state to the IL solution. To this purpose, a least-squares minimization of the EXAFS data of the 0.1 M $AgBF_4$ solution in $[C_4mim][BF_4]$ was performed with the theoretical signals employed for the $AgBF_4$ solid, by letting varying the structural parameters among the experimental uncertainties reported in Table 2. Minimization procedures have been carried out in the k-range 3.0 - 9.0 $Å^{-1}$, and the results of this fit

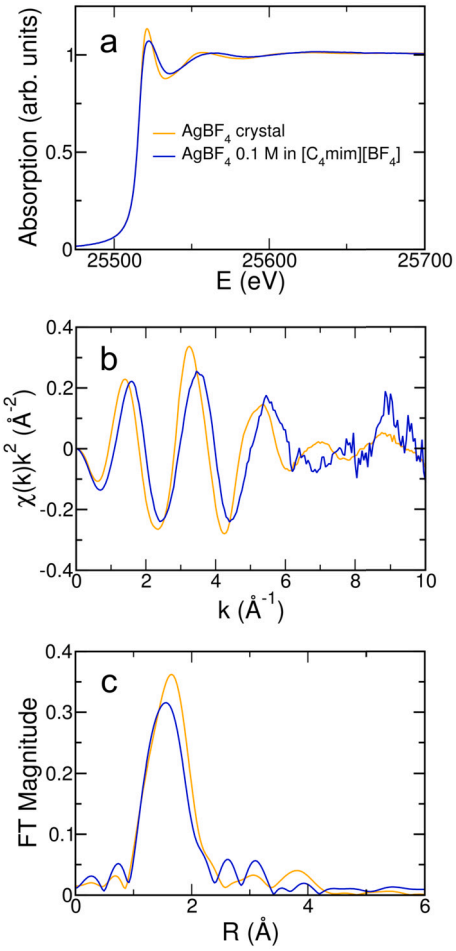

Fig. 4. Ag K-edge a) normalized XANES, b) EXAFS, and c) FT experimental spectra collected on the $AgBF_4$ salt and on the 0.1 M $AgBF_4$ solution in $[C_4mim][BF_4]$.

Table 2
Best-fit structural parameters for the Ag-F and Ag-B SS paths obtained from the analysis of the Ag K-edge EXAFS spectra collected on the $AgBF_4$ salt and on the 0.1 M $AgBF_4$ solution in $[C_4mim][BF_4]$. N is the coordination number, R the average distance, σ^2 the Debye-Waller factor, and β the asymmetry index.

	N	R (Å)	σ^2 (Å^{-2})	β
$AgBF_4$ crystal				
Ag-F^{1st}	4.0(5)	2.49(2)	0.038(2)	0.7(1)
Ag-F^{2nd}	2.0(5)	2.74(3)	0.018(3)	0.6(2)
Ag-F^{3rd}	4.0(5)	2.95(4)	0.021(4)	0.0(3)
Ag-F^{4th}	2.0(5)	3.21(4)	0.012(4)	0.0(3)
Ag-B	7.0(6)	3.64(4)	0.024(4)	0.4(3)
Ionic liquid				
Ag-F	3.9(5)	2.34(2)	0.043(4)	0.7(1)
Ag-B	3.9(6)	3.85(4)	0.050(5)	0.0(3)

are shown in Figure S1 (SM). As can be observed, the agreement between the total theoretical contribution and the experimental data is poor, as also evident from the corresponding FT's in the lower panel of Figure S1. Notably, the shorter distance of the experimental FT main peak with respect to the theoretical one is compatible with the shortening of the average Ag-F distance passing from the $AgBF_4$ salt to the IL solution. The overall result evidences that the Ag^+ ion undergoes a change in coordination when the salt is solubilized in the IL, as already suggested by the qualitative comparison of the XAS data (Fig. 4). As a

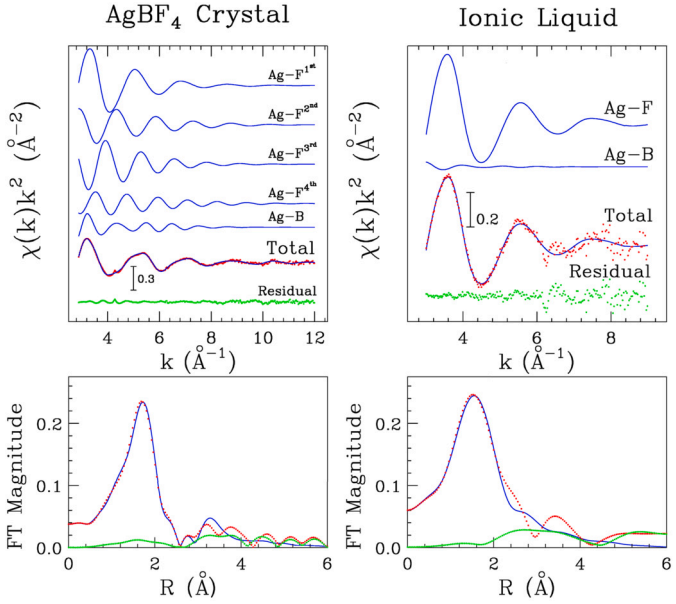

Fig. 5. Upper panels: analysis of the Ag K-edge EXAFS spectra collected on the $AgBF_4$ crystal (left panel) and on the 0.1 M $AgBF_4$ solution in $[C_4mim][BF_4]$. From the top to the bottom: Ag-F and Ag-B SS theoretical signals, total theoretical spectrum (blue line) compared with the experimental one (red dots), and the resulting residuals (green dots). Lower panels: non-phase shift corrected FT's of the best-fit EXAFS theoretical signal (blue line), of the experimental data (red dots), and of the residual curve (green dots).

consequence, in a second step the EXAFS data of the IL solution were analyzed starting from the coordination obtained from the CPMD simulation. The results of this minimization procedure are shown in the upper right panel of Fig. 5, where the two-body Ag-F and Ag-B theoretical signals are reported together with the total theoretical contribution compared with the experimental data and the resulting residuals. Note that the signals related to the distant fluorine atoms of the coordinating $[BF_4]^-$ anions have been found to provide a negligible contribution since these higher distance shells are expected to have a larger amplitude at high k-values, while the least-squares fit was performed up to 9.0 Å^{-1} due to the noise of the experimental data in the higher energy region. For the same reason, attempts of including three-body MS terms resulted in a negligible improvement of the fit quality. Nevertheless, the agreement between the theoretical and experimental data is good, as it is also evident from the corresponding FT spectra (3.0 - 9.0 Å^{-1}) shown in the lower right panel of Fig. 5. The optimized structural parameters are listed in Table 2, while the E_0 value resulted to be 1.0 eV above the first inflection point of the experimental spectrum. According to the EXAFS results, 3.9 fluorine and boron atoms are found at a 2.34(2) and 3.85(4) Å distance from the Ag^+ ion, respectively. The Ag-F distance is shorter than the one determined for the $AgBF_4$ crystal, in agreement with the qualitative comparison of the XAS data (Fig. 4), but also shorter than the one obtained from the CPMD simulation for the $AgBF_4$ solution in $[C_4mim][BF_4]$ (Fig. 1a). To get further details, we compared the Ag-F and Ag-B $g(r)$'s calculated from the CPMD simulation to the correspondent two-body distributions obtained from the EXAFS refinements, reconstructed with Γ-like functions (Figure S2). As a result, the first peak of the Ag-F $g(r)$ obtained from the CPMD method shows a compatible shape and intensity with the Ag-F distribution from the EXAFS analysis, albeit a shift towards higher distances. As concerns the Ag-B distribution, the CPMD $g(r)$ is shifted to shorter distances and also shows a more intense function with respect to the EXAFS one. This is not surprising, as DFT-based MD methods have previously observed some limitations in the description of the structural and dynamic properties of disordered liquid systems, in particular when compared with experimental data, due to the approximations introduced in this level of

theory [62,86,87]. Nevertheless, the scenarios provided by the CPMD simulation and by the EXAFS analysis are coherent in depicting an Ag^+ ion surrounded by an average number of four $[BF_4]^-$ anions in the $[C_4mim][BF_4]$ IL. In addition, the CPMD results also evidenced that a higher number of fluorine atoms is able to enter the coordination shell of the metal ion due to a fluxional binding fashion of the IL anion. This is not surprising as, although the EXAFS analysis is very sensitive towards the distance of the scattering atoms from the photoabsorber, a higher uncertainty is known to affect the determination of coordination numbers due to the high correlation with the atomic thermal and structural disorder affecting this spectral region [55]. Indeed, the Debye-Waller factor values obtained for the Ag-F and Ag-B distributions (Table 2) are relatively high if compared to those usually determined for metal ion solvation complexes [35,46,55]. This result is fully compatible with the high configurational disorder of the Ag^+ ion solvation shell as provided by the CMPD simulation, although this instance reduces the accuracy of the coordination number determination in the data analysis. To get further details, correlation effects between the coordination number and Debye-Waller factor for the Ag-F distribution have been evaluated from a correlation map between this couple of parameters, which is shown in Figure S3. As expected, a positive correlation if found between the $N_{Ag\text{-}F}$ and $\sigma^2_{Ag\text{-}F}$ values. Nevertheless, the inspection of the contours associated with a 95% confidence interval delivers an uncertainty of 3.9(5) for the Ag-F coordination number (Table 2), which is still coherent with the indication of a tetrahedral coordination.

3.3. Ag^+ ion solvation thermodynamics: classical MD results

Classical MD simulations have been carried out to obtain thermodynamic data on the Ag^+ ion solvation in $[C_4mim][BF_4]$ and for its transfer process from water. To this purpose, a new set of LJ parameters for the Ag^+ ion was developed as described in the SM. MD simulations in aqueous solution with this interaction potential were performed to obtain the thermodynamic quantities for the single-ion hydration, which are listed in Table 3 and compared with the available experimental data. The computed ΔG_{hyd} is in excellent agreement with the experimental values as determined by both Marcus [51] and Ahrland [52]. As concerns the composition of the Ag^+ ion hydration sphere, this interaction potential reproduced an Ag^+ ion coordinated by 4.0 water molecules at a Ag-O distance of 1.91 Å (Figure S5b and Table S2). This result is compatible with the commonly accepted tetrahedral model [36] and is close to the more recently proposed "2+2" one for Ag^+ ion coordination in aqueous solution [11,35]. However, the Ag-O bond distance is significantly underestimated with respect to the experimental determinations (2.31 - 2.41 Å) [35,36,46]. Any attempt of increasing the reproduced Ag-O distance resulted in an increase of the metal ion coordination number and the loss of the tetrahedral coordination geometry (see also "Generation of Ag^+ ion interaction potential" in SM). This is a known drawback of the LJ potential form that, although its simplicity and fastness, often requires compromises if one aims at simultaneous reproducing of different quantities [10,11,88,89]. In light of this, the LJ parameters developed in this work were employed, as they provide a tetrahedral coordination and a good reproduction of the experimental ΔG_{hyd}, in spite of an underestimated Ag-O bond distance. This parameter set was further tested by calculating the hydration enthalpy and entropy from free energy calculations at different temperatures. The obtained $\Delta G_{hyd}/T$ *vs*. 1/T plot is shown in Fig. 6a, while the corresponding free energy values are listed in Table S3. The calculated ΔH_{hyd} is in very good agreement with the available experimental data, in particular with Ahrland's determination (Table 3) [52]. On the other hand, the obtained ΔS_{hyd} is in excellent agreement with the direct determination provided by Marcus [90], although somewhat more negative than the value calculated from Ahrland's ΔG_{hyd} and ΔH_{hyd} [52,91].

Once validated our model in aqueous solution, we employed the same parameter set to obtain data on the Ag^+ ion solvation in $[C_4mim][BF_4]$ and for the transfer process from water to the IL. The

Table 3
MD calculated Gibbs free energy (kcal mol^{-1}) at 298 K, enthalpy (kcal mol^{-1}), and entropy (kcal mol^{-1} K^{-1}) for the Ag^+ ion hydration compared with experimental data.

	MD	Experimental
ΔG_{hyd}	-117.3 ± 0.1	-102.8 [51] -114.0 [52]
ΔH_{hyd}	-125.9 ± 0.2	-109.6† -115.4 [52]
ΔS_{hyd}	-0.029 ± 0.001	-0.023 [90] -0.005‡

† ΔH_{hyd} calculated from Marcus' ΔG_{hyd} [51] and ΔS_{hyd} [90].
‡ ΔS_{hyd} calculated from Ahrland's ΔG_{hyd} and ΔH_{hyd} [52].

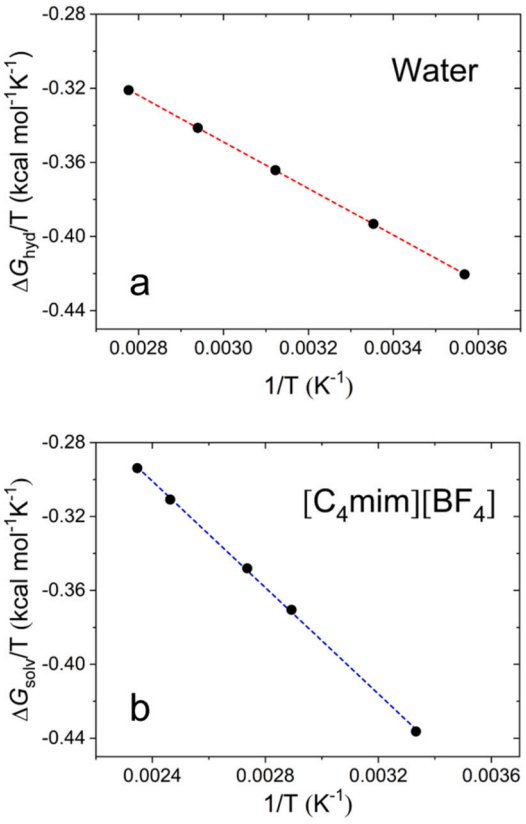

Fig. 6. $\Delta G/T$ *vs*. 1/T plots obtained for from free energy calculations at different temperatures for the Ag^+ ion in a) SPC/E water and b) $[C_4mim][BF_4]$ (R^2 = 0.99 for both regressions).

MD simulation in the IL solution delivered a Ag^+ ion surrounded by 4.2 fluorine atoms at a 1.85 Å distance, while the coordination number obtained by integration of the Ag-B $g(r)$ resulted to be 4.0 (Figure S6 and Table S4). The calculated Gibbs free energy for the single-ion solvation in $[C_4mim][BF_4]$ resulted to be -130.9 kcal mol^{-1} (Table 4). This ΔG_{solv} value is well in agreement with the available experimental data (Table S1) and is consistently less negative than those calculated previously [10,11] for the Co^{2+} and Zn^{2+} ions in the $[C_4mim][Tf_2N]$ IL with the same method (also reported in Table 4 for the sake of comparison). This result is not unsurprising, as the electrostatic contribution in the free energy is predominant [10]. It should be also noted that a tetrahedral coordination of the Ag^+ ion in the $[C_4mim][BF_4]$ IL has been obtained together with an accurate thermodynamic description, albeit an underestimated Ag-F distance with respect to the experimental one (Table 2) that derives from the known drawbacks of the LJ potential

Table 4
MD calculated Gibbs free energy (kcal mol^{-1}) at 298 K, enthalpy (kcal mol^{-1}), and entropy (kcal mol^{-1} K^{-1}) for the Ag^+ ion solvation in $[C_4mim][BF_4]$ and for the transfer from water to the IL compared with the values obtained for the Co^{2+} and Zn^{2+} ions in $[C_4mim][Tf_2N]$.†

Ion	IL	ΔG_{solv}	ΔH_{solv}	ΔS_{solv}	ΔG_{trans}(water→IL)†	ΔH_{trans}(water→IL)‡	ΔS_{trans}(water→IL)§
Co^{2+} [11]	$[C_4mim][Tf_2N]$	-451.3 ± 1.5	-507.4 ± 2.6	-0.188 ± 0.007	6.6 ± 1.6	-24.2 ± 3.2	-0.103 ± 0.009
Zn^{2+} [10]	$[C_4mim][Tf_2N]$	-441.4 ± 0.3	-538.1 ± 16.8	-0.318 ± 0.054	5.8 ± 0.5	-64.9 ± 17.2	-0.232 ± 0.055
Ag^+	$[C_4mim][BF_4]$	-130.9 ± 0.4	-143.9 ± 1.7	-0.045 ± 0.005	-13.6 ± 0.4	-18.0 ± 1.9	-0.016 ± 0.005

† ΔG_{trans}(water→IL) calculated as ΔG_{solv}(IL) - ΔG_{hyd} with the values reported in Table 3 for hydration.
‡ ΔH_{trans}(water→IL) calculated as ΔH_{solv}(IL) - ΔH_{hyd} with the values reported in Table 3 for hydration.
§ ΔS_{trans}(water→IL) calculated as ΔS_{solv}(IL) - ΔS_{hyd} with the values reported in Table 3 for hydration.

form. The overall result confirms the reliability of the employed parameters set and simulation protocol also for the IL case. The obtained ΔG_{solv} is more negative than the calculated ΔG_{hyd} (Table 3), delivering a negative free energy for the transfer process of the Ag^+ ion from water to $[C_4mim][BF_4]$. Indeed, the calculated ΔG_{trans}(water→IL) of -13.6 kcal mol^{-1} (Table 4) is in agreement with the experimental ones (Table 1) and confirms that the Ag^+ ion is more favorably solvated in the IL than in water. It is worth stressing that this result shows an opposite trend with respect to the Co^{2+} and Zn^{2+} ions, for which the transfer process from water to the $[C_4mim][Tf_2N]$ IL was found to be unfavorable because of positive ΔG_{trans}(water→IL) (Table 4).

To get further insights, the enthalpic and entropic contributions to the ΔG_{solv} were obtained by means of free energy calculations at variable temperature (Fig. 6b, data in Table S5). The obtained ΔH_{solv} and ΔS_{solv} values are both negative (Table 4), as usually observed for metal ion solvation processes, due to the breaking of the solvent-solvent interactions and the solvent ordering around the solute [92]. The solvation enthalpy and entropy in the IL are both more negative than the correspondent values in water (Table 3), and thus also the transfer functions are both negative. Previously, similar studies performed for the Co^{2+} and Zn^{2+} ions in $[C_4mim][Tf_2N]$ gave much more negative ΔH_{trans}(water→IL) (Table 4) as expected on the basis of the stronger electrostatic interaction of the divalent metal ions with the IL as compared to water [10,11]. However, in those cases, largely negative ΔS_{trans}(water→IL) values were also obtained, this being the unfavorable contribution to the transfer process leading to positive ΔG_{trans}(water→IL). For the Ag^+ ion in $[C_4mim][BF_4]$ a slightly negative ΔS_{trans}(water→IL) is obtained as well, showing that also in this case the entropic contribution opposes to the transfer process. However, the enthalpic term prevails and the transfer process results to be thermodynamically favored (negative ΔG_{trans}(water→IL)). This finding suggests that, although the ordering effect imposed by the Ag^+ ion in $[C_4mim][BF_4]$ is still higher than in water, it is smaller than that exerted by the Co^{2+} and Zn^{2+} ions in the $[C_4mim][Tf_2N]$ IL.

The overall picture subtends a wide horizon of interpretations. On one hand, the less negative ΔS_{trans}(water→IL) can be assigned to the lower charge of the monovalent Ag^+ ion, which imposes a lower ordering effect on the IL structure in comparison to Co^{2+} and Zn^{2+}. Also, the lower coordination number of the Ag^+ ion, which is surrounded by four $[BF_4]^-$ anions, implies a smaller loss of disorder upon formation of the solvated complex compared to the octahedral Co^{2+} and Zn^{2+} cases, for which the arrangement of six $[Tf_2N]^-$ anions in the metal ion coordination sphere was determined previously [10,11]. In addition, the configurational disorder of the Ag^+ ion solvation sphere in $[C_4mim][BF_4]$ as determined by the CPMD simulation and by the EXAFS analysis could play a role in the entropic contribution. Finally, also the different structural nature of the anions should be considered, namely: the relatively rigid $[BF_4]^-$ anion loses less degrees of freedom than the flexible $[Tf_2N]^-$ upon coordination to the metal ion. Altogether these instances demonstrate in which terms the higher solvating capability of the $[BF_4]^-$ anion is declined. As far as the Ag^+ in $[C_4mim][BF_4]$ is concerned, we demonstrated that its more favorable solvation relies on a different enthalpy-entropy compensation with respect to divalent metal ions.

4. Conclusions

Overall, the structural and thermodynamic results reported in this work provide a picture of a disordered local environment around the Ag^+ ion in the $[C_4mim][BF_4]$ IL, where the coordinating $[BF_4]^-$ anions present an internal dynamics leading to different binding modes and, at the same time, can be exchanged with the bulk.

CPMD simulations show that in $[C_4mim][BF_4]$ the Ag^+ ion is coordinated by an average number of four $[BF_4]^-$ anions in a roughly tetrahedral geometry, at variance with the $AgBF_4$ salt. Moreover, the anions exchange observed in the CPMD trajectory allows to hypothesize the presence of the $[Ag(BF_4)_3]^{2-}$ species in solution due to a solvational equilibrium with the outer-sphere solvent, which should have a preferential olefin uptake with respect to $[Ag(BF_4)_4]^{3-}$. EXAFS data analysis evidenced that the $[C_4mim][BF_4]$ IL is able to dissolve the $AgBF_4$ salt giving rise to a different coordination with respect to the solid state, and confirmed the tetrahedral model provided by the CPMD method.

The Gibbs free energy for the transfer of the Ag^+ ion from water to $[C_4mim][BF_4]$ derived from classical MD is in good agreement with the available experimental data, and confirms the metal ion as more favorably solvated in the IL than in aqueous solution. The negative transfer free energy is opposite from that previously calculated for divalent ions in ILs carrying the same cation and the $[Tf_2N]^-$ anion, for which the ΔG_{trans}(water→IL) was positive. The spontaneous transfer process of the Ag^+ ion is driven by the enthalpic term and disfavored by the negative ΔS_{trans}(water→IL). Nevertheless, the enthalpy-entropy compensation responsible for the favorable transfer can be explained by the lower ordering of the solvent imposed by the monovalent Ag^+ ion, which is tetrahedrally coordinated in $[C_4mim][BF_4]$, with respect to the divalent ions, but also to the more rigid structure of the $[BF_4]^-$ anion with respect to the $[Tf_2N]^-$ case.

CRediT authorship contribution statement

Matteo Busato: Conceptualization, Formal analysis, Investigation, Writing – original draft, Writing – review & editing. **Paola D'Angelo:** Formal analysis, Investigation, Writing – review & editing. **Andrea Lapi:** Investigation. **Francesco Tavani:** Investigation. **Daniele Veclani:** Investigation. **Marilena Tolazzi:** Funding acquisition, Investigation, Writing – review & editing. **Andrea Melchior:** Conceptualization, Formal analysis, Funding acquisition, Investigation, Project administration, Resources, Software, Supervision, Writing – original draft, Writing – review & editing.

Declaration of competing interest

The authors declare that they have no known competing financial interests or personal relationships that could have appeared to influence the work reported in this paper.

Data availability

Data will be made available on request.

Acknowledgements

We acknowledge Elettra Sincrotrone Trieste S.C.p.A. and its staff for providing synchrotron radiation beam time and laboratory facilities (proposal n. 20190065). Part of the calculations were performed on the Galileo system of the CINECA supercomputing center (grant IsC80_MBAg-202 - HP10CBK4BN). This work was supported by the University of Udine in the framework of the Strategic Plan 2022-25 – Interdepartmental Research Project ESPeRT.

References

[1] R. Hayes, G.G. Warr, R. Atkin, Structure and nanostructure in ionic liquids, Chem. Rev. 115 (13) (2015) 6357–6426, https://doi.org/10.1021/cr500411q.
[2] X. Han, D.W. Armstrong, Ionic liquids in separations, Acc. Chem. Res. 40 (11) (2007) 1079–1086, https://doi.org/10.1021/ar700044y.
[3] M. Regel-Rosocka, M. Wisniewski, Ionic liquids in separation of metal ions from aqueous solutions, in: S. Handy (Ed.), Applications of Ionic Liquids in Science and Technology, IntechOpen, Rijeka, 2011, Ch. 18.
[4] R.B. Gujar, P.K. Verma, B. Mahanty, A. Bhattacharyya, S.M. Ali, R.J. Egberink, J. Huskens, W. Verboom, P.K. Mohapatra, Sequestration of Np^{4+} and NpO_2^{2+} ions by using diglycolamide-functionalized azacrown ethers in C_8mim·NTf_2 ionic liquid: extraction, spectroscopic, electrochemical and DFT studies, J. Mol. Liq. 370 (2023) 120872, https://doi.org/10.1016/j.molliq.2022.120872.
[5] H. Niu, L. Wang, P. Guan, N. Zhang, C. Yan, M. Ding, X. Guo, T. Huang, X. Hu, Recent advances in application of ionic liquids in electrolyte of lithium ion batteries, J. Energy Storage 40 (2021) 102659, https://doi.org/10.1016/j.est.2021.102659.
[6] D.R. MacFarlane, N. Tachikawa, M. Forsyth, J.M. Pringle, P.C. Howlett, G.D. Elliott, J.H. Davis, M. Watanabe, P. Simon, C.A. Angell, Energy applications of ionic liquids, Energy Environ. Sci. 7 (2014) 232–250, https://doi.org/10.1039/C3EE42099J.
[7] Q. Zhang, Q. Wang, S. Zhang, X. Lu, X. Zhang, Electrodeposition in ionic liquids, ChemPhysChem 17 (3) (2016) 335–351, https://doi.org/10.1002/cphc.201500713.
[8] M. Armand, F. Endres, D. MacFarlane, H. Ohno, B. Scrosati, Ionic-liquid materials for the electrochemical challenges of the future, Nat. Mater. 8 (2009) 621–629, https://doi.org/10.1038/nmat2448.
[9] P. Wasserscheid, Transition metal catalysis in ionic liquids, in: Handb. Green Chem., American Cancer Society, 2010, pp. 65–91, Ch. 3.
[10] M. Busato, P. D'Angelo, A. Melchior, Solvation of Zn^{2+} ion in 1-alkyl-3-methylimidazolium bis(trifluoromethylsulfonyl)imide ionic liquids: a molecular dynamics and X-ray absorption study, Phys. Chem. Chem. Phys. 21 (2019) 6958–6969, https://doi.org/10.1039/C8CP07773H.
[11] M. Busato, P. D'Angelo, A. Lapi, M. Tolazzi, A. Melchior, Solvation of Co^{2+} ion in 1-butyl-3-methylimidazolium bis(trifluoromethylsulfonyl)imide ionic liquid: a molecular dynamics and X-ray absorption study, J. Mol. Liq. 299 (2020) 112120, https://doi.org/10.1016/j.molliq.2019.112120.
[12] M. Busato, A. Lapi, P. D'Angelo, A. Melchior, Coordination of the Co^{2+} and Ni^{2+} Ions in Tf_2N^- based ionic liquids: a combined X-ray absorption and molecular dynamics study, J. Phys. Chem. B 125 (24) (2021) 6639–6648, https://doi.org/10.1021/acs.jpcb.1c03395.
[13] A. Melchior, C. Gaillard, S. Gràcia Lanas, M. Tolazzi, I. Billard, S. Georg, L. Sarrasin, M. Boltoeva, Nickel(II) complexation with nitrate in dry [C_4mim][Tf_2N] ionic liquid: a spectroscopic, microcalorimetric, and molecular dynamics study, Inorg. Chem. 55 (7) (2016) 3498–3507, https://doi.org/10.1021/acs.inorgchem.5b02937.
[14] J.M. Hartley, C.-M. Ip, G.C.H. Forrest, K. Singh, S.J. Gurman, K.S. Ryder, A.P. Abbott, G. Frisch, EXAFS study into the speciation of metal salts dissolved in ionic liquids and deep eutectic solvents, Inorg. Chem. 53 (12) (2014) 6280–6288, https://doi.org/10.1021/ic500824r.
[15] S. Takemura, S. Kawakami, M. Harada, M. Iida, Solvation structure of a copper(II) ion in protic ionic liquids comprising N-hexylethylenediamine, Inorg. Chem. 53 (18) (2014) 9667–9678, https://doi.org/10.1021/ic501177t.
[16] P.-P. Sun, H.-I. Song, T.-Y. Kim, B.-J. Min, S.-Y. Cho, Recovery of silver from the nitrate leaching solution of the spent Ag/α-Al_2O_3 catalyst by solvent extraction, Ind. Eng. Chem. Res. 53 (52) (2014) 20241–20246, https://doi.org/10.1021/ie5041918.
[17] S. Laki, A. Arabi Shamsabadi, F. Seidi, M. Soroush, Sustainable recovery of silver from deactivated catalysts using a novel process combining leaching and emulsion liquid membrane techniques, Ind. Eng. Chem. Res. 57 (41) (2018) 13821–13832, https://doi.org/10.1021/acs.iecr.8b02933.
[18] U. Domańska, A. Rękawek, Extraction of metal ions from aqueous solutions using imidazolium based ionic liquids, J. Solution Chem. 38 (6) (2009) 739–751, https://doi.org/10.1007/s10953-009-9402-7.
[19] K. Shimojo, M. Goto, Solvent extraction and stripping of silver ions in room-temperature ionic liquids containing calixarenes, Anal. Chem. 76 (17) (2004) 5039–5044, https://doi.org/10.1021/ac049549x.
[20] G.-T. Wei, Z. Yang, C.-J. Chen, Room temperature ionic liquid as a novel medium for liquid/liquid extraction of metal ions, Anal. Chim. Acta 488 (2) (2003) 183–192, https://doi.org/10.1016/S0003-2670(03)00660-3.
[21] A. Basile, A.I. Bhatt, A.P. O'Mullane, S.K. Bhargava, An investigation of silver electrodeposition from ionic liquids: influence of atmospheric water uptake on the silver electrodeposition mechanism and film morphology, Electrochim. Acta 56 (7) (2011) 2895–2905, https://doi.org/10.1016/j.electacta.2010.12.083.
[22] D. Depuydt, N.R. Brooks, S. Schaltin, L. VanMeervelt, J. Fransaer, K. Binnemans, Silver-containing ionic liquids with alkylamine ligands, ChemPlusChem 78 (6) (2013) 578–588, https://doi.org/10.1002/cplu.201300063.
[23] J.G.d.R. d. Costa, J.M. Costa, A.F.d. Almeida Neto, Progress on electrodeposition of metals and alloys using ionic liquids as electrolytes, Metals 12 (12) (2022) 2095, https://doi.org/10.3390/met12122095.
[24] T. Ren, M. Patel, K. Blok, Olefins from conventional and heavy feedstocks: energy use in steam cracking and alternative processes, Energy 31 (4) (2006) 425–451, https://doi.org/10.1016/j.energy.2005.04.001.
[25] Z. Lei, W. Arlt, P. Wasserscheid, Separation of 1-hexene and n-hexane with ionic liquids, Fluid Phase Equilib. 241 (1) (2006) 290–299, https://doi.org/10.1016/j.fluid.2005.12.024.
[26] Y. Cheng, F. Li, Q. Wu, K. Peng, B. Fan, Y. Bai, Z. Wang, N. Zhang, X. Zhang, Efficient ethylene/ethane separation by rare earth metal-containing ionic liquids in N,N-dimethylformamide, Sep. Purif. Technol. 310 (2023) 123094, https://doi.org/10.1016/j.seppur.2023.123094.
[27] D.J. Safarik, R.B. Eldridge, Olefin/paraffin separations by reactive absorption: a review, Ind. Eng. Chem. Res. 37 (7) (1998) 2571–2581, https://doi.org/10.1021/ie970897h.
[28] C.M. Sanchez, T. Song, J.F. Brennecke, B.D. Freeman, Hydrogen stable supported ionic liquid membranes with silver carriers: propylene and propane permeability and solubility, Ind. Eng. Chem. Res. 59 (12) (2020) 5362–5370, https://doi.org/10.1021/acs.iecr.9b04886.
[29] S. Park, O. Morales-Collazo, B. Freeman, J.F. Brennecke, Ionic liquid stabilizes olefin facilitated transport membranes against reduction, Angew. Chem., Int. Ed. 61 (25) (2022) e202202895, https://doi.org/10.1002/anie.202202895.
[30] X. Wu, X. Li, L. Xu, W. He, Z. Zhou, W. Liu, F. Zhang, Z. Ren, Application of silver ionic liquid in the separation of olefin and alkane, J. Chem. Technol. Biotechnol. 97 (5) (2022) 1207–1214, https://doi.org/10.1002/jctb.7009.
[31] Q. Wu, G. Li, Y. Cheng, B. Fan, Y. Bai, N. Zhang, Z. Wang, X. Zhang, S. Zhang, Efficient separation of ethylene/ethane by incorporation of silver salts into protic imidazole ionic liquids, Chem. Eng. J. 461 (2023) 141942, https://doi.org/10.1016/j.cej.2023.141942.
[32] A. Ortiz, A. Ruiz, D. Gorri, I. Ortiz, Room temperature ionic liquid with silver salt as efficient reaction media for propylene/propane separation: absorption equilibrium, Sep. Purif. Technol. 63 (2) (2008) 311–318, https://doi.org/10.1016/j.seppur.2008.05.011.
[33] P. Eor, D. Ryoo, H. Nan, J.L. Anderson, Characterizing olefin selectivity and stability of silver salts in ionic liquids using inverse gas chromatography, ACS Omega 5 (48) (2020) 31362–31369, https://doi.org/10.1021/acsomega.0c04854.
[34] P. Eor, J.L. Anderson, Using a chromatographic pseudophase model to elucidate the mechanism of olefin separation by silver(I) ions in ionic liquids, Anal. Chem. 93 (39) (2021) 13284–13292, https://doi.org/10.1021/acs.analchem.1c02885.
[35] I. Persson, K.B. Nilsson, Coordination chemistry of the solvated silver(I) ion in the oxygen donor solvents water, dimethyl sulfoxide, and N,N'-dimethylpropyleneurea, Inorg. Chem. 45 (18) (2006) 7428–7434, https://doi.org/10.1021/ic060636c.
[36] Y. Tsutsui, K.-i. Sugimoto, H. Wasada, Y. Inada, S. Funahashi, EXAFS and ab initio molecular orbital studies on the structure of solvated silver(I) ions, J. Phys. Chem. A 101 (15) (1997) 2900–2905, https://doi.org/10.1021/jp963792l.
[37] N. Prasetyo, Y. Hidayat, Lability of the first solvation shell of silver cations in liquid ammonia: a quantum mechanical charge field molecular dynamics simulation study, J. Mol. Liq. 350 (2022) 118517, https://doi.org/10.1016/j.molliq.2022.118517.
[38] P.L. Zanonato, P. Di Bernardo, A. Melchior, M. Tolazzi, P. Polese, M. Busato, Solvent and structural effects on silver(I) complex formation: thermodynamics and modeling, J. Therm. Anal. Calorim. 147 (9) (2022) 5501–5509, https://doi.org/10.1007/s10973-021-11071-z.
[39] P. Luigi Zanonato, P. Di Bernardo, A. Melchior, M. Busato, M. Tolazzi, Lanthanides(III) and silver(I) complex formation with triamines in DMSO: the effect of ligand cyclization, Inorg. Chim. Acta 503 (2020) 119392, https://doi.org/10.1016/j.ica.2019.119392.
[40] P.L. Zanonato, A. Melchior, M. Busato, P. Di Bernardo, M. Tolazzi, Silver(I) complexes with long-chain diamines in non-aqueous solvents, J. Therm. Anal. Calorim. 138 (5) (2019) 3257–3265, https://doi.org/10.1007/s10973-019-08725-4.
[41] A. Melchior, M. Tolazzi, P. Polese, P.L. Zanonato, Thermodynamics of complex formation of silver(I) with N-donor ligands in non-aqueous solvents, J. Therm. Anal. Calorim. 130 (1) (2017) 461–469, https://doi.org/10.1007/s10973-017-6289-1.
[42] A. Melchior, E. Peralta, M. Valiente, C. Tavagnacco, F. Endrizzi, M. Tolazzi, Interaction of d^{10} metal ions with thioether ligands: a thermodynamic and theoretical study, Dalton Trans. 42 (2013) 6074–6082, https://doi.org/10.1039/C3DT32332C.
[43] S. Del Piero, R. Fedele, A. Melchior, R. Portanova, M. Tolazzi, E. Zangrando, Solvation effects on the stability of silver(I) complexes with pyridine-containing ligands studied by thermodynamic and DFT methods, Inorg. Chem. 46 (11) (2007) 4683–4691, https://doi.org/10.1021/ic070124d.
[44] A. Melchior, M. Sanadar, R. Cappai, M. Tolazzi, Entropy and enthalpy effects on metal complex formation in non-aqueous solvents: the case of silver(I) and monoamines, Entropy 24 (9) (2022), https://doi.org/10.3390/e24091253.
[45] J.R. Pliego, Car-Parrinello molecular dynamics study of CuF, AgF, $CuPF_6$ and $AgPF_6$ in acetonitrile solvent and cluster-continuum calculation of the solvation free energy

of Cu(I), Ag(I) and Li(I), J. Mol. Liq. 359 (2022) 119368, https://doi.org/10.1016/j.molliq.2022.119368.
[46] M. Busato, A. Melchior, V. Migliorati, A. Colella, I. Persson, G. Mancini, D. Veclani, P. D'Angelo, Elusive coordination of the Ag^+ ion in aqueous solution: evidence for a linear structure, Inorg. Chem. 59 (23) (2020) 17291–17302, https://doi.org/10.1021/acs.inorgchem.0c02494.
[47] T.A. Pham, C. Horwood, A. Maiti, V. Peters, T. Bunn, M. Stadermann, Solvation properties of silver and copper ions in a room temperature ionic liquid: a first-principles study, J. Phys. Chem. B 122 (50) (2018) 12139–12146, https://doi.org/10.1021/acs.jpcb.8b10559.
[48] M. Imai, I. Tanabe, Y. Ozaki, K. Fukui, Solvation properties of silver ions in ionic liquids using attenuated total reflectance ultraviolet spectroscopy, J. Mol. Liq. 364 (2022) 119998, https://doi.org/10.1016/j.molliq.2022.119998.
[49] A. Lewandowski, I. Stepniak, Relative molar Gibbs energies of cation transfer from a molecular liquid to ionic liquids at 298.15 K, Phys. Chem. Chem. Phys. 5 (2003) 4215–4218, https://doi.org/10.1039/B305734H.
[50] A. Lewandowski, M. Osinska, I. Stepniak, Stability of Ag^+ complexes with cryptand 222 in ionic liquids, J. Incl. Phenom. 52 (3–4) (2005) 237–240, https://doi.org/10.1007/s10847-004-7242-z.
[51] Y. Marcus, Thermodynamics of solvation of ions. Part 5.—Gibbs free energy of hydration at 298.15 K, J. Chem. Soc. Faraday Trans. 87 (18) (1991) 2995–2999, https://doi.org/10.1039/FT9918702995.
[52] S. Ahrland, Solvation and complex formation - competing and cooperative processes in solution, Pure Appl. Chem. 54 (8) (1982) 1451–1468.
[53] R. Spezia, C. Nicolas, A. Boutin, R. Vuilleumier, Molecular dynamics simulations of a silver atom in water: evidence for a dipolar excitonic state, Phys. Rev. Lett. 91 (2003) 208304, https://doi.org/10.1103/PhysRevLett.91.208304.
[54] C.M. Blauth, A.B. Pribil, B.R. Randolf, B.M. Rode, T.S. Hofer, Structure and dynamics of hydrated Ag^+: an ab initio quantum mechanical/charge field simulation, Chem. Phys. Lett. 500 (4) (2010) 251–255, https://doi.org/10.1016/j.cplett.2010.10.008.
[55] A. Filipponi, P. D'Angelo, XAS in Liquid Systems, John Wiley I& Sons, Ltd, 2016, pp. 745–771, Ch. 25.
[56] P. D'Angelo, G. Chillemi, V. Barone, G. Mancini, N. Sanna, I. Persson, Experimental evidence for a variable first coordination shell of the cadmium(II) ion in aqueous, dimethyl sulfoxide, and N,N'-dimethylpropyleneurea solution, J. Phys. Chem. B 109 (18) (2005) 9178–9185, https://doi.org/10.1021/jp050460k.
[57] CPMD v4.3 copyright IBM corp 1990–2019, copyright MPI fuer Festkoerperforschung Stuttgart 1997–2001.
[58] S. Grimme, Semiempirical GGA-type density functional constructed with a long-range dispersion correction, J. Comput. Chem. 27 (15) (2006) 1787–1799, https://doi.org/10.1002/jcc.20495.
[59] L. Kleinman, D.M. Bylander, Efficacious form for model pseudopotentials, Phys. Rev. Lett. 48 (1982) 1425–1428, https://doi.org/10.1103/PhysRevLett.48.1425.
[60] J.C. Grossman, E. Schwegler, E.W. Draeger, F. Gygi, G. Galli, Towards an assessment of the accuracy of density functional theory for first principles simulations of water, J. Chem. Phys. 120 (1) (2004) 300–311, https://doi.org/10.1063/1.1630560.
[61] E. Schwegler, J.C. Grossman, F. Gygi, G. Galli, Towards an assessment of the accuracy of density functional theory for first principles simulations of water. II, J. Chem. Phys. 121 (11) (2004) 5400–5409, https://doi.org/10.1063/1.1782074, arXiv:cond-mat/0405561.
[62] P. D'Angelo, V. Migliorati, F. Sessa, G. Mancini, I. Persson, XANES reveals the flexible nature of hydrated strontium in aqueous solution, J. Phys. Chem. B 120 (17) (2016) 4114–4124, https://doi.org/10.1021/acs.jpcb.6b01054.
[63] R. Spezia, M. Duvail, P. Vitorge, T. Cartailler, J. Tortajada, G. Chillemi, P. D'Angelo, M.-P. Gaigeot, A coupled Car-Parrinello molecular dynamics and EXAFS data analysis investigation of aqueous Co^{2+}, J. Phys. Chem. A 110 (48) (2006) 13081–13088, https://doi.org/10.1021/jp064688z.
[64] S. Amira, D. Spångberg, V. Zelin, M. Probst, K. Hermansson, Car-Parrinello molecular dynamics simulation of Fe^{3+}(aq), J. Phys. Chem. B 109 (29) (2005) 14235–14242, https://doi.org/10.1021/jp050186u.
[65] M. Bühl, S. Grigoleit, H. Kabrede, F.T. Mauschick, Simulation of ^{59}Co NMR chemical shifts in aqueous solution, Chem. Eur. J. 12 (2) (2006) 477–488, https://doi.org/10.1002/chem.200500285.
[66] M.M. Taib, T. Murugesan, Density, refractive index, and excess properties of 1-butyl-3-methylimidazolium tetrafluoroborate with water and monoethanolamine, J. Chem. Eng. Data 57 (1) (2012) 120–126, https://doi.org/10.1021/je2007204.
[67] F. Sessa, V. Migliorati, A. Serva, A. Lapi, G. Aquilanti, G. Mancini, P. D'Angelo, On the coordination of Zn^{2+} ion in Tf_2N^- based ionic liquids: structural and dynamic properties depending on the nature of the organic cation, Phys. Chem. Chem. Phys. 20 (2018) 2662–2675, https://doi.org/10.1039/C7CP07497B.
[68] W. Humphrey, A. Dalke, K. Schulten, VMD: visual molecular dynamics, J. Mol. Graph. 14 (1996) 33–38.
[69] M. Brehm, B. Kirchner, TRAVIS - a free analyzer and visualizer for Monte Carlo and molecular dynamics trajectories, J. Chem. Inf. Model. 51 (8) (2011) 2007–2023, https://doi.org/10.1021/ci200217w.
[70] L. Martínez, R. Andrade, E.G. Birgin, J.M. Martínez, PACKMOL: a package for building initial configurations for molecular dynamics simulations, J. Comput. Chem. 30 (13) (2009) 2157–2164, https://doi.org/10.1002/jcc.21224.
[71] J.N. Canongia Lopes, J. Deschamps, A.A. Pádua, Modeling ionic liquids using a systematic all-atom force field, J. Phys. Chem. B 108 (6) (2004) 2038–2047, https://doi.org/10.1021/jp0362133.
[72] Z. Liu, S. Huang, W. Wang, A refined force field for molecular simulation of imidazolium-based ionic liquids, J. Phys. Chem. B 108 (34) (2004) 12978–12989, https://doi.org/10.1021/jp048369o.
[73] M.J. Abraham, T. Murtola, R. Schulz, S. Páll, J.C. Smith, B. Hess, E. Lindahl, GROMACS: high performance molecular simulations through multi-level parallelism from laptops to supercomputers, SoftwareX 1–2 (2015) 19–25, https://doi.org/10.1016/j.softx.2015.06.001.
[74] C.H. Bennett, Efficient estimation of free energy differences from Monte Carlo data, J. Comput. Phys. 22 (2) (1976) 245–268, https://doi.org/10.1016/0021-9991(76)90078-4.
[75] J. Carlsson, J. Åqvist, Calculations of solute and solvent entropies from molecular dynamics simulations, Phys. Chem. Chem. Phys. 8 (2006) 5385–5395, https://doi.org/10.1039/B608486A.
[76] J. Carlsson, J. Åqvist, Absolute hydration entropies of alkali metal ions from molecular dynamics simulations, J. Phys. Chem. B 113 (30) (2009) 10255–10260, https://doi.org/10.1021/jp900818z.
[77] A.D. Cicco, G. Aquilanti, M. Minicucci, E. Principi, N. Novello, A. Cognigni, L. Olivi, Novel XAFS capabilities at ELETTRA synchrotron light source, J. Phys. Conf. Ser. 190 (1) (2009) 012043, https://doi.org/10.1088/1742-6596/190/1/012043.
[78] A. Filipponi, A. Di Cicco, X-ray-absorption spectroscopy and *n*-body distribution functions in condensed matter. I. Theory, Phys. Rev. B 52 (21) (1995) 15122–15134, https://doi.org/10.1103/PhysRevB.52.15135.
[79] A. Filipponi, A. Di Cicco, X-ray-absorption spectroscopy and *n*-body distribution functions in condensed matter. II. Data analysis and applications, Phys. Rev. B 52 (21) (1995) 15135–15149, https://doi.org/10.1103/PhysRevB.52.15135.
[80] L. Hedin, S. Lundqvist, Effects of electron-electron and electron-phonon interactions on the one-electron states of solids, Solid State Phys. 23 (1970) 1–181, https://doi.org/10.1016/S0081-1947(08)60615-3.
[81] E. Burattini, P. D'Angelo, A. Di Cicco, A. Filipponi, N.V. Pavel, Multiple scattering x-ray absorption analysis of simple brominated hydrocarbon molecules, J. Phys. Chem. 97 (21) (1993) 5486–5494, https://doi.org/10.1021/j100123a007.
[82] E. Goreshnik, Z. Mazej, X-ray single crystal structure and vibrational spectra of $AgBF_4$, Solid State Sci. 7 (10) (2005) 1225–1229, https://doi.org/10.1016/j.solidstatesciences.2005.06.007.
[83] B. Ravel, ATOMS: crystallography for the X-ray absorption spectroscopist, J. Synchrotron Radiat. 8 (2) (2001) 314–316, https://doi.org/10.1107/S090904950001493X.
[84] D.-e. Jiang, S. Dai, First principles molecular dynamics simulation of a task specific ionic liquid based on silver olefin complex: atomistic insights into a separation process, J. Phys. Chem. B 112 (33) (2008) 10202–10206, https://doi.org/10.1021/jp801914k.
[85] I. Persson, 2.19 - coordination chemistry of metal ions in some oxygen donor solvents, in: E.C. Constable, G. Parkin, L. Que Jr (Eds.), Comprehensive Coordination Chemistry III, Elsevier, Oxford, 2021, pp. 352–367.
[86] V. Pham, I. Tavernelli, C. Milne, R. van der Veen, P. D'Angelo, C. Bressler, M. Chergui, The solvent shell structure of aqueous iodide: X-ray absorption spectroscopy and classical, hybrid QM/MM and full quantum molecular dynamics simulations, Chem. Phys. 371 (1) (2010) 24–29, https://doi.org/10.1016/j.chemphys.2010.03.023.
[87] R. Spezia, M. Duvail, P. Vitorge, T. Cartailler, J. Tortajada, G. Chillemi, P. D'Angelo, M.P. Gaigeot, A coupled Car-Parrinello molecular dynamics and EXAFS data analysis investigation of aqueous Co^{2+}, J. Phys. Chem. A 110 (48) (2006) 13081–13088, https://doi.org/10.1021/jp064688z.
[88] P. Li, B.P. Roberts, D.K. Chakravorty, K.M.J. Merz, Rational design of particle mesh Ewald compatible Lennard-Jones parameters for +2 metal cations in explicit solvent, J. Chem. Theory Comput. 9 (6) (2013) 2733–2748, https://doi.org/10.1021/ct400146w.
[89] P. Li, L.F. Song, K.M. Merz, Systematic parameterization of monovalent ions employing the nonbonded model, J. Chem. Theory Comput. 11 (4) (2015) 1645–1657, https://doi.org/10.1021/ct500918t.
[90] Y. Marcus, A. Loewenschuss, Standard entropies of hydration of ions, Annu. Rep. Prog. Chem., Sect. C, Phys. Chem. 81 (1984) 81–135, https://doi.org/10.1039/PC9848100081, Chapter 4.
[91] S. Ahrland, Complex equilibria, solvation and solubility, Pure Appl. Chem. 62 (11) (1990) 2077–2082.
[92] P. Di Bernardo, A. Melchior, R. Portanova, M. Tolazzi, P.L. Zanonato, Complex formation of N-donor ligands with group 11 monovalent ions, Coord. Chem. Rev. 252 (10–11) (2008) 1270–1285, https://doi.org/10.1016/j.ccr.2007.12.007.